Durability

of

BioGrout

Hanna Dura

Deltares, department of Geo- Engineering, Delft, Netherlands

TABLE OF CONTENTS

LIST OF PICTURES, FIGURES AND TABLES

LIST OF SYMBOLS

d	diameter
h	height
h_{prec}	precipitated height
K	permeability
m	mass
m_{sat}	saturated mass
m_{dry}	dry mass
N	number of cycles
N_f	number of cycles upon failure
q	stress, strength
q_{cyc}	cyclic strength
q_{max}	peak strength
q_{min}	minimum strength
q_{pre}	predicted strength with respect to dry density
q_1	peak strength at 1:1 ratio
$q_{0.5}$	peak strength at 1:2 ratio
V	volume
V_{mat}	matrix volume
V_{por}	pore volume
ϕ	porosity
ρ	density
ρ_{dry}	dry density

1 INTRODUCTION

BioGrout is a new promising material to be used for ground improving purposes based on microbial induced precipitation of carbonate by urea hydrolysis. Previously performed large scale experiments and subsequent tests on compressive strength give promising results, especially with regard to the fact that BioGrout can be created with various strengths. The process of cementation can be controlled in order to yield a strength desired for a specific application. However the long term effects on BioGrout in regard to mechanical requirements imposed by civil engineering applications and exposure to chemical processes in the subsurface are not yet known. In order to determine the behavior of BioGrout once exposed in a specific environment laboratory tests were conducted.

One of the possible applications of BioGrout is the strengthening of weak railroad embankments. This application will subject the ground material to repeated load and unload phases as trains will pass. This work gives a first insight on the long term performance of biologically precipitated sand when subjected to cyclic loading with respect to degradation of stiffness and loss of strength. The test was performed on five different cyclic load amplitudes with up to 52.000 cycles.

Like natural sandstones also BioGrout will be exposed to chemical alteration through percolating rain water as well as ground water. Important factors of durability regarding the properties of natural sandstones, which of course also apply to BioGrout, are the mineral composition, texture and cementation. Since the cementation in BioGrout is biologically induced there are slight differences in the cementation properties (van Paassen 2009). Therefore the effect of pore fluids on the cementation and thus strength properties might differ from natural sandstones. To identify the effect of pore fluids on the strength of BioGrout several samples have been continuously flushed with 260 pore volumes of demineralized water and artificial rain water and subsequently their compressive strength evaluated. With the correlation of van Paassen (2009) between compressive strength and dry density the residual strength of the treated samples was estimated.

Another aspect challenging the durability of ground materials is being induced by weather conditions. Therefore an additional experiment that has been carried out in regard to the durability of BioGrout included the effect of freezing and thawing cycles on the compressive strength. But since extreme cold phases are rather unlikely to occur in the regions where BioGrout is most likely to be applied, the effect of this aspect on the durability is rather negligible.

2 MECHANICAL DURABILITY

BioGrout has the potential to rise up to an alternative ground improvement method increasing strength and stiffness of loose, high compressible soils. This is especially of interest for railroad embankments that consist of such layers of soft highly compressible soil, as it often is the case in the Netherlands. These tracks demand continuous monitoring and maintenance in order to prevent any damage and further hazardous situations. Regarding the time and costs of the current maintenance of weak embankments, it is desirable to find a technique for reinforcement that to UMGEHEN this.

The already conducted tests on the peak strength of BioGrout during monotonic loading show very promising results. However passing trains subject the underlying soil to permanently repeated load and unload phases. This repeating load unload cycles might have a very different affect on the long term strength than already performed monotonic loading.

In order to shed more light on this question of durability when subjected to dynamic loading, samples of the second field scale experiment of BioGrout have been subjected to cyclic loading. The cores have been subjected to load amplitudes typical for civil engineering applications. A train imposes a load of approximately 60kPa on the embankment when passing by. The conducted tests were performed with loading phases up to 100kPa as starting value and unloading phases to 10kPa in each cycle. The vertical stress imposed on the samples was increased each hour until a maximum value of 1400kPa was reached, on which the experiment was kept running for a maximum time of 72 hours or upon premature failure of the sample. This high load is true to be far outside the range the material would encounter in civil engineering applications, nevertheless it can give a better more rapid insight on the process of degradation of stiffness.

For real live application we have to take into account the weight i.e. the load of a passing by train, the frequency of the load unload cycles during passing, the number of wagons and number of axes respectively and speed at which the train is travelling. Also important is the number of trains passing by throughout the day and year. Since not all trains have the same properties regarding number of axes, weight, length and velocity only a very brief overall estimation can be made here. The results presented are sufficient to give a trend of behavior of the material at cyclic loading, which can be used for further more specific applications.

2.1 MATERIAL

The tests on the mechanical durability of the biologically cemented sand were conducted on samples obtained from the second field scale experiment at Papendrecht (Picture 2.1). In this procedure a concrete container (8.0m x 5.6m x 1.5m) was filled with Itterbeck sand (Smals IKW) under wet conditions with an average dry density of 1560 kg/m^3. The procedure of precipitation was carried out on the basis of the first field scale experiment with some modifications stated **in the field report**.

Ten cores were drilled from one block located approximately in front of injection point 1on the bottom of the container, from which five samples were taken for cyclic triaxial tests (Picture 2.2 and 2.3). The exact dimensions of the samples can be found in table 2.1. The samples were cut from the drilled cores in a way to obtain the maximum homogeneity in each sample.

PICTURE 2.1: Container from the second field scale experiment at Papendrecht.

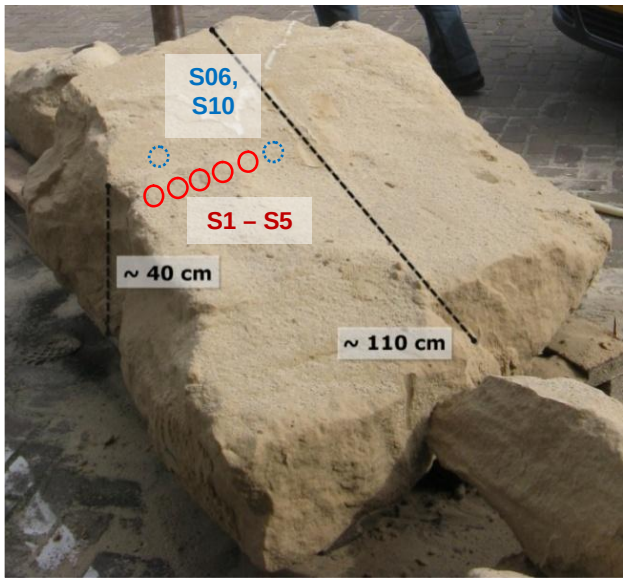

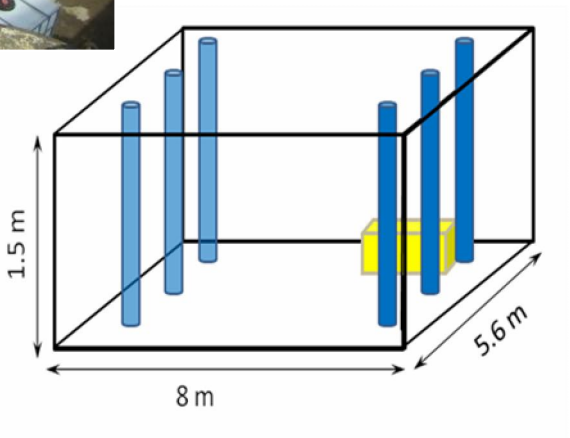

PICTURE 2.2: Sketch of location of the block from which the cores for testing have been drilled, as shown on the left.

PICTURE 2.3: Block from second field scale experiment. Indicated are the locations of the five samples tested under cyclic loading (S1-S5) and freeze- thaw cycles (S06,S10).

TABLE 2.1: Dimensions and properties of tested samples.

		S 1	S 2	S 3	S 4	S 5
h	[cm]	13.55	13.69	12.68	13.23	12.78
d	[cm]	6.27	6.4	6.41	6.39	6.38
m_{sat}	[g]	860.33	911.8	868.24	899.31	840.86
V_i	[cm^3]	418.37	440.41	405.12	424.28	408.57
ρ_{sat}	[g/m^3]	2.056	2.070	2.143	2.12	2.06
ρ_{dry}	[g/m^3]	1.693	1.867	1.836	1.794	1.669
ϕ_{dry}	[%]	36.36	29.82	30.72	32.55	36.12
K_i		2.45E-05	1.43E-05	1.84E-05	1.85E-05	9.96E-06
$CaCO_3$ cont.	[mg/cm^3]	39.99	40.12	56.26	51.67	50.49

2.2 CYCLIC TRIAXIAL LOADING

Although a lot of research has been conducted on stress- strain behavior of various kinds of geomaterials, giving a good understanding of ground movement patterns, more specific investigations on the degradation of stiffness of calcareous soils are omitted, especially with consideration of cyclic loading. Thus the data available for the durability of calcareous soils when subjected to cyclic loading is very limited. Moreover since BioGrout is a biologically precipitated sand the cementation of the material is not the exact same as in naturally precipitated sandstones, which might cause differences in its mechanical properties.

In the course of this work the behavior and thus durability of BioGrout under long lasting cyclic loading has been investigated according to the procedures stated below. Subjects of main importance of this research were the driving forces and patterns of degradation of stiffness with the emphasis on how long the biologically precipitated sand can withstand unload reload cycles as for example are imposed by passing trains.

2.2.1 TEST PROCEDURE

The cyclic triaxial test was performed on 5 samples from the second field experiment as previously stated. The samples were fully saturated by applying a back pressure until the B- value reached at least 0.96 according to standards. Throughout the course of the test a constant confining pressure of 50kPa was applied. The test was performed under undrained conditions. The frequency of the load unload cycle was set on 0.2 Hz, with a total test duration of approximately 72 h, which makes for ca. 52.000 cycles. The load unload cycles were chosen to alternate between initially 10 and 100kPa with an increase of load amplitude every hour by doubling until reaching a final load amplitude of 1400kPa which was kept constant for the rest of the test (details can be seen in table. 2.2). During cyclic loading the vertical applied force, vertical displacement, pore pressure as well as cell pressure were continuously measured with a sampling rate of 0.37 seconds, making for 13 sampling points per cycle.

For samples that did not fail within 72h of the test the cyclic loading was stopped and monotonic loading was initiated upon failure. The monotonic loading was conducted in the same triaxial cell, so that the samples did not have to be moved.

2.2.2 DOCUMENTATION

In the following a brief overview of the test procedures and details of the properties of the samples will be given. It is important to say that Sample 5, which was tested as the first one did not undergo the exact same procedure as the following samples. The time scheme of all tested samples can be found in table 2.2. Initially a maximum load amplitude of 100kPa was chosen according to forces implied in civil engineering applications as previously discussed. After a test duration of 70h of S5, still no major effects on the sample could be observed from the recorded data. Therefore the load amplitude was increased successively until a maximum amplitude of 1400kPa.
Hence the following testing was carried out with the same starting load amplitude but the increase in loads was increased each hour during the initial 4h of the test by doubeling until reaching again the maximum load amplitude of 1400kPa, on which the test was kept running to the end.

TABLE 2.2: Time scheme of increasing loads for all tested samples

	Stress	S 1	S 2	S 3	S 4	S 5
Step 1:	100 [kPa]	0 - 60	0 – 70	0 - 60	0 -60	0 - 4165
Step 2:	200 [kPa]	60 - 120	70 – 156	60 - 120	60 - 120	4165 - 4566
Step 3:	400 [kPa]	120 - 180	156 - 216	120 - 183	120 - 183	4566 - 4641
Step 4:	800 [kPa]	180 - 223	216 - 240	183 - 245	183 - 249	4641 - 4676
Step 5:	1400 [kPa]		240 - 2584	245 - 4320	249 - 3150	4676 - 5929
time of failure [h,min]		**3h, 43 min**	**43h, 4min**	**72h**	**52h, 30 min**	**98h, 49min**

TABLE 2.3: Details of cyclic triaxial tests performed on BioGrout samples, including estimation of peak strength

		S 1	S 2	S 3 *	S 4	S 5 *
q_{est}	[kPa]	902.883	2564.690	2129.394	1655.060	781.795
q_{cyc}	[kPa]	800	1400	1400	1400	1400
q_{max}	[kPa]	800	1400	2447.33	1400	657.28
N_f	[-]	2660	30530	51840	37800	71148

* did not fail during cyclic loading

Table 2.3 shows the cyclic and in some cases monotonic strength along with the number of cycles upon failure. It also contains the predicted monotonic strength which was calculated for the samples according to the correlation of van Paassen (2009). But it is important to mention here that this correlation cannot hold for the cyclic loading since the

type of load application is distinctive for the behavior of the material tested. This can be very well seen in S5. During cyclic loading S5 was able to withstand a load amplitude of 1400kPa over approximately 20h of cyclic loading. However during subsequent monotonic loading the sample failed already at a load of approximately 660kPa.

2.3 RESULTS AND DISCUSSION

The data was mainly processed in IGOR Pro 5.01 to determine the deformation characteristics of the material during the cyclic loading. The main focus of interpretation was the verification of the stress- strain behavior as well as degradation of stiffness in terms of change in shear modulus and the driving factors and patterns of the degradation.

2.3.1 STIFFNESS PROPERTIES

In theory a soil subjected to cyclic loading will respond with so a called hysteresis to this kind of stress pattern (O'Reilly and Brown, 1991). During the course of the experiment the stress- strain curves showed this characteristically hysteresis behavior with increasing number of cycles. Fig. 2.1 shows the stress- strain relation of S3 during cyclic loading for the initial 20.000 cycles (approx. 28h), representatively for all the conducted tests, since the behavior was very similar for all samples. The jumps in the stress level depict the increases of loads each hour. As the data processed in this graph is very dense the single ellipses are not visible, however a constant creep across the strain axis can be clearly seen, thus indicating a damping of the material. The deformation of the sample, especially regarding the lower loads of 100 or 200 kPa, that represent the stress levels induced by civil engineering applications, is in the range of only 0.01 to 0.02%, which already indicates the high stiffness of the material.

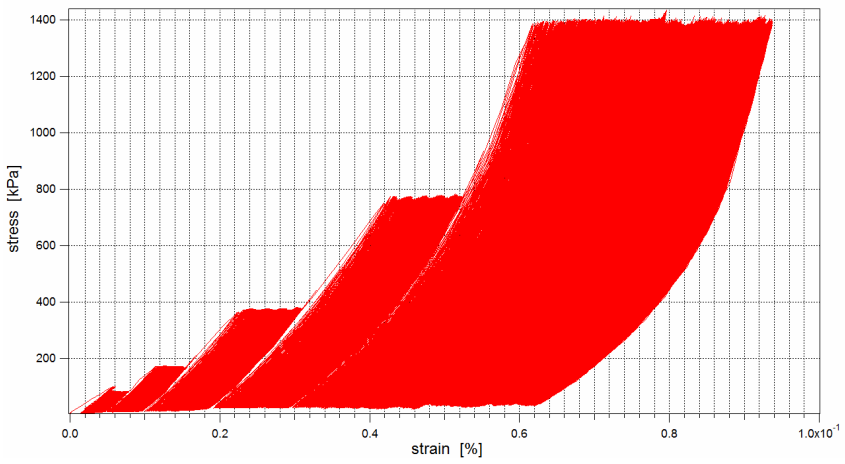

FIGURE 2.1: Stress- strain behavior of S3 for initial 20.000 cycles

Figures 2.2 and 2.3 show only few single ellipses with a constant interval of 100 cycles and 2500 cycles respectively in order to illustrate the development of the hysteresis with increasing nmber of cycles and applied cyclic load amplitudes. As can be seen from the first graph, showing the development of the hysteresis for the load levels of 100, 200 and 400kPa, the increase in strain becomes smaller with increasing number of cycles in each load

level. This behavior shows that on low loads the material becomes stiffer with increasing number of cycles. Fig. 2.3 shows the same for the load amplitude of 1400kPa. Here it appears that the creep of the hysteresis along the strain axis shows only a very small increase until a sudden jump by approximately 0.8% of strain causing the sample to fail. This behavior shows that it is rather hard to predict the failure of the samples since there are no strong signs of increasing weakening of the sample. As soon as the material reaches over to the plastic zone it fails very rapidly. As can also be seen in figure 2.4 the deformation of the material is extremely low. Tests of all samples have shown that the displacement in all cases has only reached a maximum range of approximately 1-2 mm before failure. S3 and S5, which did not fail during cyclic loading show an even lower displacement of only 1.4 mm and 0.18 mm respectively. From this follows that the material can withstand relatively high cyclic loads throughout a long period of time. However once the deformation exceeds a certain point the material fails very rapidly not giving room for any plastic deformation.

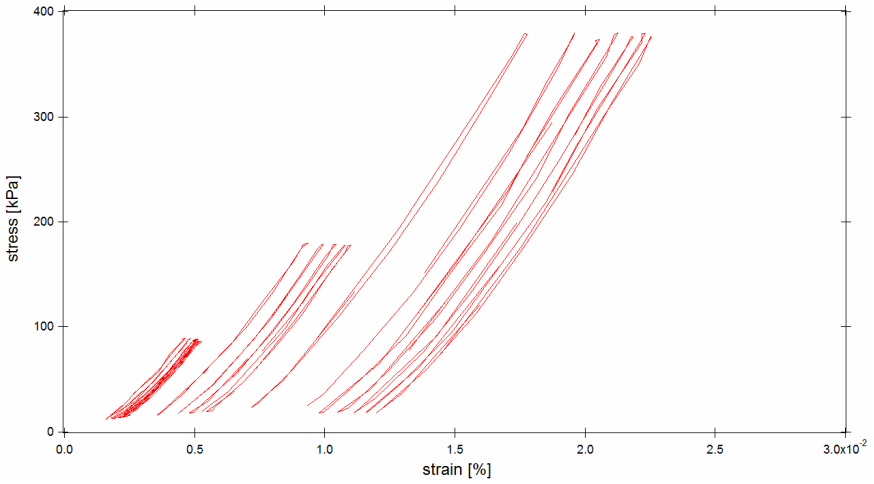

FIGURE 2.2: Stress- strain behavior of S2, showed for load amplitudes of 100kPa, 200kPa and 400kPa, with a constant interval of 100 cycles

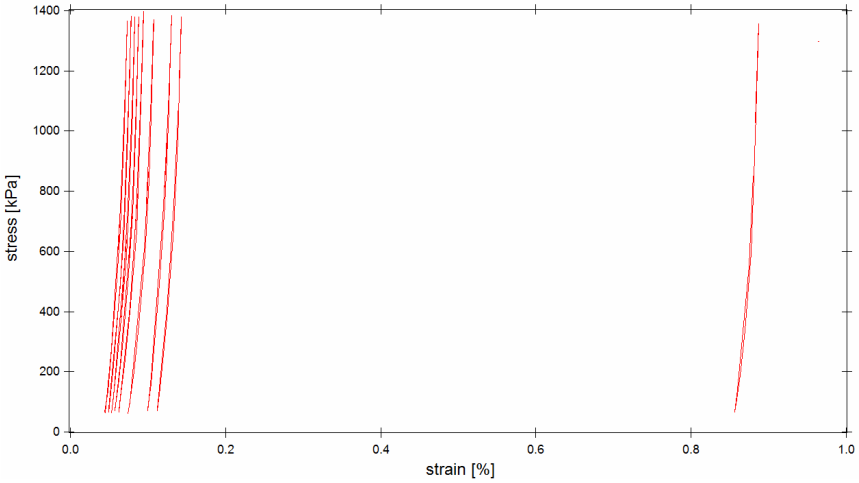

FIGURE 2.3: Stress- strain behavior of S2, showed for load amplitude 1400kPa with a constant interval of 2.500 cycles

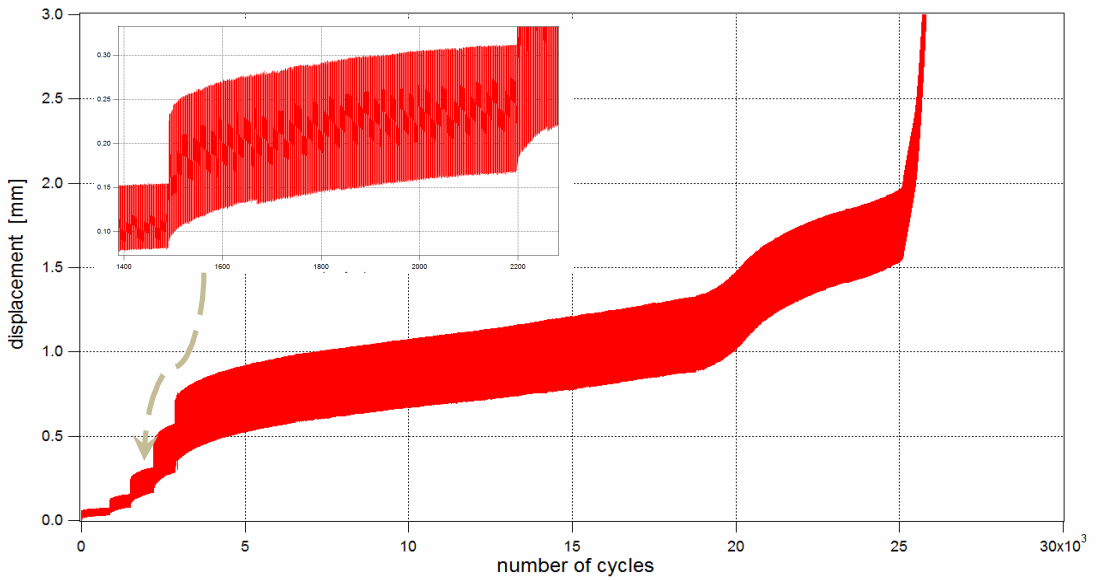

FIGURE 2.4: Displacement with increasing number of cycles upon failure for S2, with a zoom on the increase of displacement on load amplitude 400kPa.

2.3.2 FATIGUE BEHAVIOR

In the previous chapter we have already seen that the material does not only show a simple stiff behavior with increasing number of cycles, but seems to become stiffer with time on a low cyclic load amplitude. The actual failure or first signs of fatigue behavior of the samples occurred on a multiple level of load amplitude of those to be used in real civil engineering applications with a rather sudden event as was seen in Fig. 2.3. This can be confirmed by further examinations of the shear modulus, which was calculated according to figure. 2.5.

The deviator stress q has been calculated according to $q=(\sigma_1-\sigma_3)$ with σ_1 and σ_3 the major and minor principal stresses. Regarding single loops the deviatory cyclic stress q_c was obtained as stated in figure 2.5. Since the cyclic loading has been conducted under undrained conditions the shear strain ε_s is equal to the main strain ε_1.

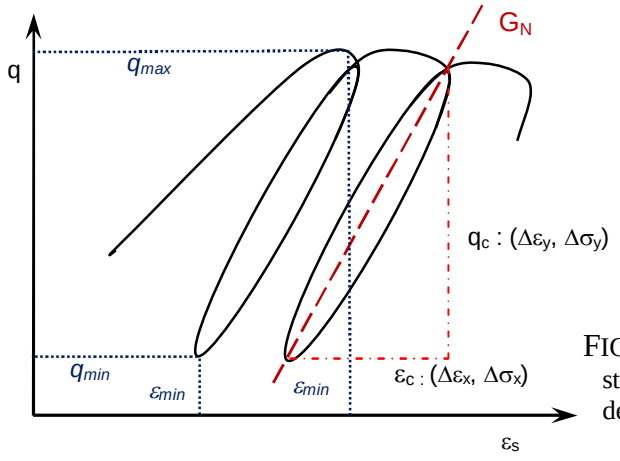

FIGURE 2.5: Scheme of calculating G- Modulus from stress- strain diagram, with Gn as the shear modulus depending on the number of cycles

In order to make further examinations on the fatigue behavior first the unload reload paths of a single cycle regarding the shear modulus and deviatoric strain should be compared, as shown in Fig 2.6. For practical reasons only a few data points for the reloading part are available, but never the less it can be seen from the graph, that the unload and reload parts of a cycle follow the same path. Therefore in the following discussions on the fatigue behavior of the material it will not be distinguished between unload and reload parts of one cycle, considering both parts follow the same path. Merely the reloading part obviously reaches higher values, that way a wider range of values can be covered.

Bearing this in mind the shear modulus, and thus the stiffness can be further examined in this manner. Fig. 2.7 (A) and (B) show the development of the shear modulus in regard to vertical applied stress for four and three cycles respectively. The values in these graphs have been picked to show the range of the initial 700 cycles on 100kPa vertical stress (A) and the range of the last cycles before failure on 1400kPa (B). From this a clear change in shear modulus with increasing stress and number of cycles can be seen. In both plots, i.e. on the minimum and maximum vertical stress applied the shear modulus follows a linear trend within each loop. However during minimum stress application the slope of the trendlines for subsequent cycles is nearly identical and the distance between them seems to show a small decrease with increasing number of cycles. On the other hand in Fig. 2.7 (B) showing the same correlation for the maximum applied stress it can be seen that the behavior of the shear modulus with respect to the applied stress and number of cycles has changed. Overall the amplitude of the shear modulus as well as the slope of the trendline, which previously has been observed to be constant, has decreased and shows a further decrease with increasing number of cycles on this particular stress level.

The correlation between shear modulus, applied stress and number of cycles found here corresponds with the previously shown stress- strain graphs. On the minimum applied stress level the slope of the curves is maximal and the distance between them shows a small decreasing trend in subsequent cycles. This means the stiffness increases within one cycle during the loading part of the cycle and falls back to a lower value on the subsequent cycle. However the decrease of stiffness on subsequent cycles seems to decline with increasing number of cycles. During maximum applied stress the shear modulus and thus the stiffness of the material is decreasing rapidly.

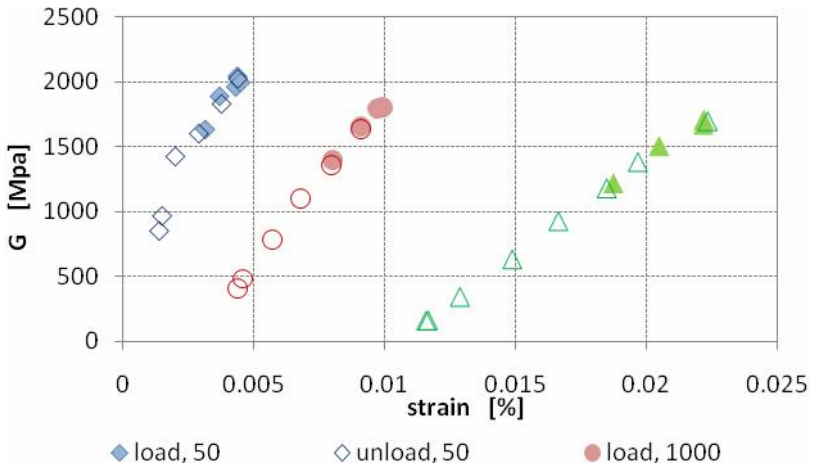

FIGURE 2.6: Shear modulus for unload- reload parts of loops regarding to strain for S2, for 100kPa (blue), 200kPa (red) and 400kPa (green).

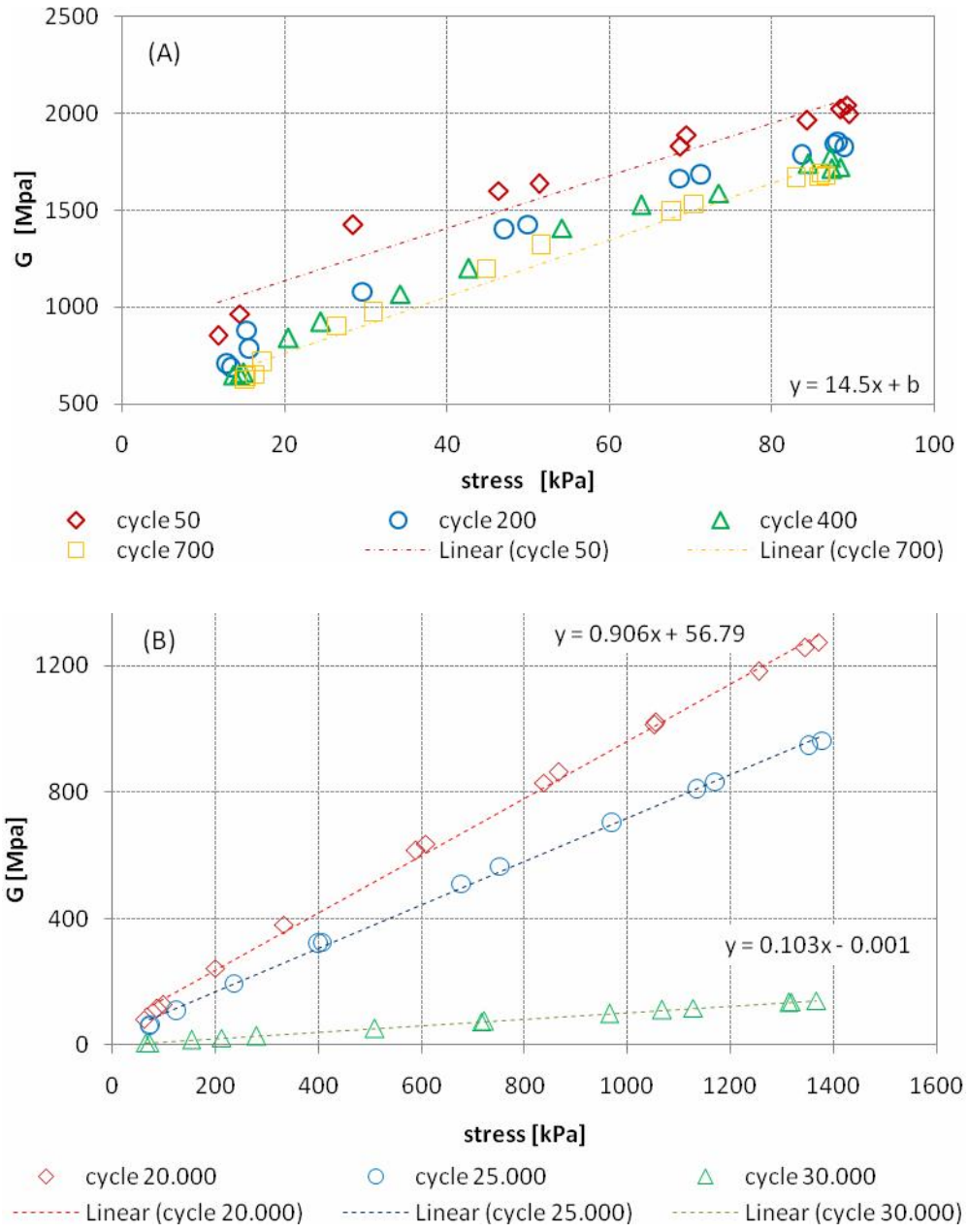

FIURE 2.7: Development of shear modulus against stress with increasing number of cycles for S2 at (A) 100kPa and (B) 1400kPa load amplitude.

This behavior will be further examined in terms of the shear modulus in a cycle N (G_N) with respect to the shear modulus of the very first cycle (G_1) considered over the entire range of cycles the samples were subjected to. The degradation curves in Figure 2.8 are shown for S1 and S3, the weakest and the strongest sample, in order to demonstrate the different dimensions of stiffness and its degradation, which are never the less following the same trend. From Figure 2.8 (A), showing the weakest sample tested, it can be clearly observed that the shear modulus within one load amplitude remains on a relatively constant level with only minor variations, which are most probably due to intergranuler movements. This means that even with increasing number of cycles on a comparably low stress level the material does not undergo very significant changes in stiffness. Only within the last increase of load amplitude, which eventually led to failure of the sample, there is an immediate decrease in G_N observable. Each increase in vertical stress yields also a jump like increase in

shear modulus, indicating a stiffer behavior on higher applied loads. Figure 2.8 (B) shows the same relationship for S3, with a very similar behavior as S1. The inlet zooms into the section of the figure at low ratios of G_N/G_1 revealing the same pattern as already seen for S1. As we can see from further comparison with S1, the range of shear modulus on low stress amplitudes is close to zero, yet shows the same jumps in G_N/G_1 as the vertical stress was increased. However with the load increase to 1400kPa there is a very great increase in G_N with eventually decreasing values with increasing number of cycles, thus indicating the degradation of stiffness of this sample at that point.

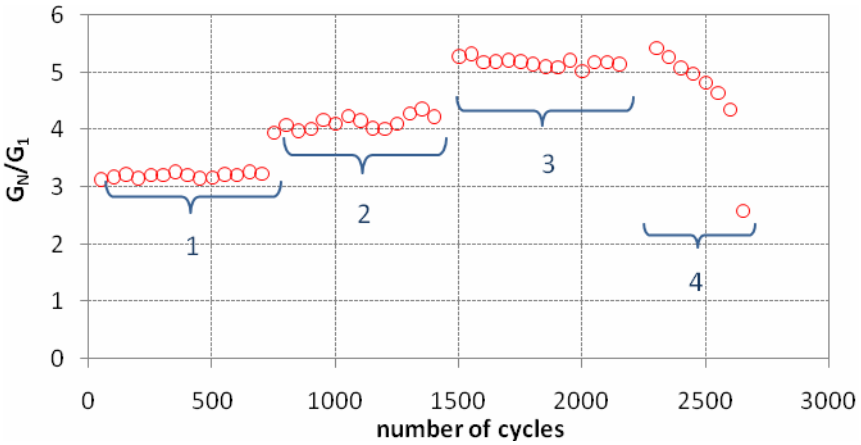

1: load: 100kPa, cycles 50-700;
2: load: 200kPa, cycles 750-1400;
3: load: 400kPa, cycles 1500-2150
4: load: 800kPa, cycles 2300-2650
All intervals: 50

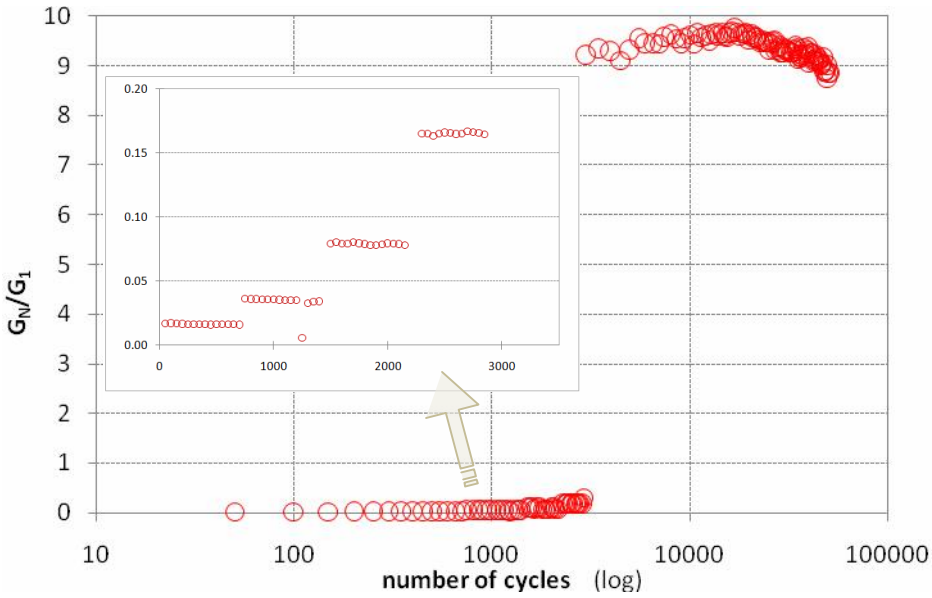

Inlet: Zoom of low load levels shown on the bottom of the graph with same parameters as in figure 2.8 (A). Data points in top right of the main graph are corresponding to G_N/G_1 for load amplitude 1400kPa, interval: 500

FIGURE 2.8: Degradation of stiffness as shear modulus of cycle N (G_N) with respect to initial shear modulus (G_1), with increasing number of cycles for S3 (A) and S1 (B).

From the shown correlations it is hard to distinguish what effect exactly the number of cycles has on the stiffness of the material. Hence for further investigation the cyclic shear strain ε_c is shown against the number of cycles in figure 2.9. For low cyclic loads ε_c follows a slowly decreasing pattern, which remains more or less constant on the initial three cyclic load amplitudes. The last increase to 800kPa shows an increase of strain with increasing number of cycles following an exponential trendline, eventually causing the sample to fail.

From this it can be understood that on relatively low cyclic loads the strain of the material is decreasing in a very slow but stable manner throughout the entire time on a particular load. However it can be speculated that the strain will not continue to decrease indefinitely but will reach a yield value from which it will remain constant or start to raise. On higher loads such as in the ending phase of the test of this sample an immediate phase of softening is encountered. This correlation holds representatively for all other samples subjected to cyclic loading.

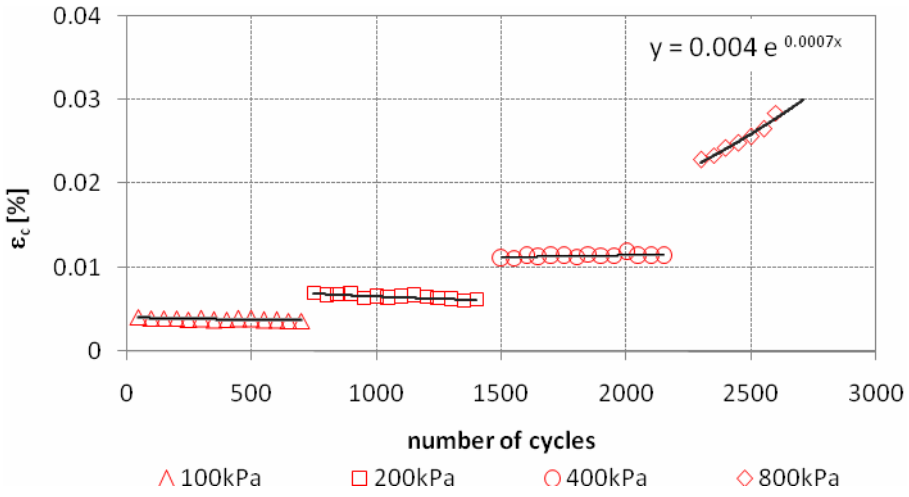

FIGURE 2.9: Strain within one cycle with respect to number of cycles for S1.

Since the strain is the driving factor of the stability of the material the normalized shear modulus (G_N/G_1) was plotted against the cyclic strain (ε_c) as shown in figure 2.10. The degradation curves in (A) are plotted for S1, S2, S4 and S5 at cyclic load amplitudes of 100kPa to 800kPa for cycles 50-2900 with an interval of 50 cycles and at load amplitude 1400kPa cycles 3000 upon failure with an interval of 500 cycles except for S5 with an interval of 1000 cycles at that load amplitude. Figure 2.10 (B) is a zoom of the degradation curve for S1, S2 and S4 at load amplitude 100kPa. It can be seen from the plots that all samples follow more or less the same pattern in degradation of stiffness. The vertical stress put on the samples obviously does not significantly influence the pattern of stiffness degradation. With each increase of vertical stress there is obviously a jump like increase in shear modulus, as well as strain, as already seen in previous figures. However the following decrease of it with increasing strain follows the same pattern. As can be seen from 2.10 (B) on a low cyclic stress level, as is of interest in civil engineering applications, the degradation of stiffness follows an entirely linear trend. It can be observed, that with a higher initial stiffness its degradation occurs on a steeper slope with increasing strain, than a lower initial stiffness would encounter.

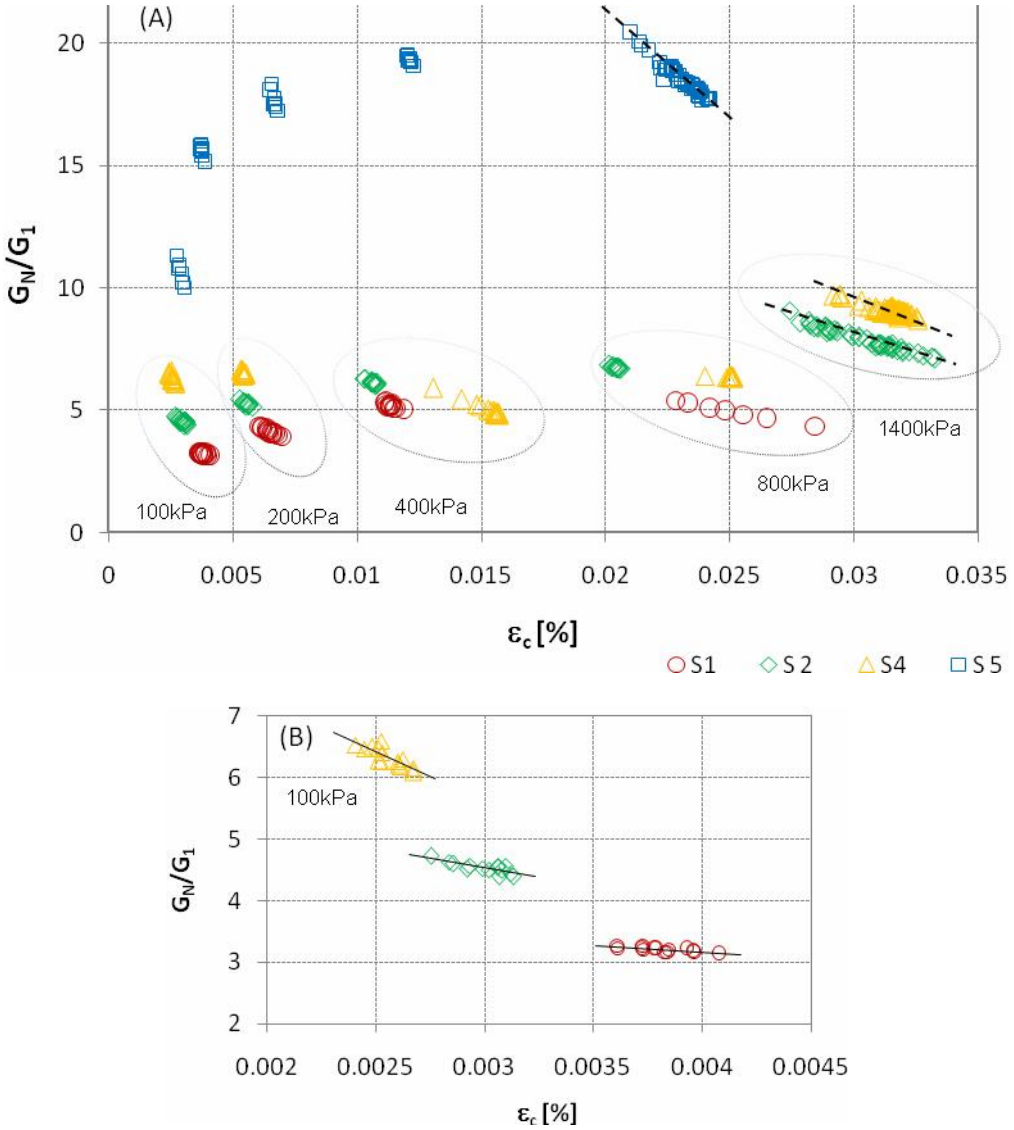

FIGURE 2.10: (A) Degradation of stiffness with respect to cyclic shear strain and number of cycles, (B) shows zoom into the degradation curves of S1, S2 and S4 on load amplitude 100kPa for initial 700 cycles.

However the data does not show any yield value of strain separating the initial stiffness from a start of substantial stiffness degradation as reported by Sharma and Fahey (2003). As can be seen from the presented data the tested BioGrout shows a clearly linear response to cyclic loading throughout all tested cyclic load amplitudes and number of cycles. Therefore it will be rather hard to distinguish and predict at which point the degradation of stiffness will be high enough to cause failure.

2.4 SUMMARY AND CONCLUSION

An initial investigation on the mechanical durability of biologically precipitated sand was made. Conclusively it can be said that within the range of civil engineering applications the material shows very good results regarding its durability. From the presented graphs it follows that when subjected to cyclic loads as a passing train would enduce on the material, its respond is an elastic behavior with extremly small values of decrease in stiffness throughout a number of cycles of up to approximately 50.000. Only on extremely high cyclic loads as high as 1400kPa the material starts to reach over to the plastic zone where failure occurres very rapidly. The common observation, as stated by Sharman and Fahey (2004), that there is only little effect on stiffness with increasing number of cycles after reaching a particular number of cycles, is found not to hold for dry sands, as Lo Presti et al. (1997) suggested. However during this research the BioGrout samples have been subjected to a very high number of cycles on different loads showing an overall very stable continuous decrease of stiffness for the lower applied loads, e.i. 100-800kPa. The material seems to reach into the plastic zone rather suddenly where failure occures very rapidly due to the high sitffness of the material that does not allow for any plasitc deformation.

3 CHEMICAL DURABILITY

The chemical durability of biologically precipitated sands is an important aspect regarding its final application possibilities. As tests regarding chemical durability are mainly being conducted on building material and regarding the fact that these materials do not encounter any kind of fluid flow inside their pores, research data on this topic is very limited.

As BioGrout has the potential to be used as a ground improvement material for rail road embankments to name one example not only the mechanical durability regarding cyclic loading is of interest, as was presented in the first part of this work. Also its resistance to chemical alteration regarding the degradation of strength is an important aspect that needs to be investigated. Particularly in the Netherlands this will play an important role since the groundwater level is overall very high. Therefore the main goal of this part of the study was to give a first insight on the degradation of strength of this material through chemical alteration. Particularly in regard to ground water flow and percolating rain water five samples of BioGrout, specifically made for this purpose according to standards stated in M. P. Harkes et al. (2009), were flushed with 260 pore volumes of demineralized water and artificial rain water respectively, demonstrating the worst case scenario a soil could encounter. Monitoring the dissolution of $CaCO_3$ in the effluents, along with sub sequentially performed UCS tests and the correlation of van Paassen (2009) between peak strength and dry density, it was possible to estimate the residual strength of the treated material

With an average ground water flow rate through natural sandstones of appxorimately 1 m/day the flow rate chosen for this experiment was approx. 140 times higher. With the amount of flushed fluid through the sand columns and the higher flow rate the following data can be correlated with 20 years of groundwater flow through BioGrout. Since the process of dissolution is a simple linear trend these values can be extrapolated to even longer times.

3.1 MATERIAL

The BioGrout was specifically made for the purpose of the chemical durability tests according to the procedure stated by M. P. Harkes et al. (2009). Five PVC tubes with an internal diameter of 6.6 cm and a total length of 18 cm were packed with approximately 1 cm of filter sand on top and bottom of each column and 16 cm of fine Itterbeck sand between the filter sand layers (figure 3.1). All columns were treated in a full saturated state, flushing the fluids from top to bottom. Details of the sand columns as they were packed as well as the actual precipitated height of the precipitated sand bodies can be seen in table 3.1.

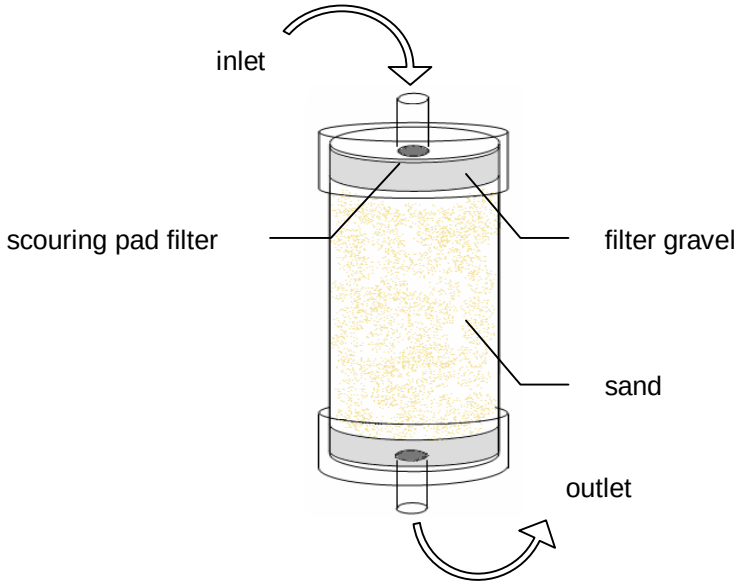

FIGURE 3.1: Sketch of column set up for precipitation and flushing procedure.

A bacterial suspension with an optical density of 2.50 (OD_{600}) and an activity of 1.75mS/cm was at first flushed through the sand columns to about one fourth of the pore volume. Immediately after placing the bacteria, 100 ml of 50mM $CaCl_2$ fixation fluid was flushed through each column in order to prevent loss of bacteria in sub sequential flushing. After fixing the bacteria the cementation fluid, containing 1 M of $CaCl_2$ and urea was flushed in several batches, approximately with 250 ml per batch and column. The first batch of cementation fluid was flushed through immediately after inserting the fixation fluid. A second batch of cementation fluid was flushed through after a 2h reaction time. After this the sand columns were left for another reaction time of 24h until the third batch was flushed. The fourth batch was flushed through the columns after a reaction time of 7h.

During the time of precipitation the ammonium concentration of the effluents was measured as an indicator of bacterial activity and thus creation of $CaCO_3$. Samples were taken during each flush of cementation fluid at different times. 2 ml of sample were added to a cuvette containing 100µl of Nessler reagent. After a reaction time of 1 min the optical density of the sample was measured in a spectrophotometer at 425nm. Readings indicated a good conversion rate of $CaCO_3$.

TABLE 3.1: Details of packed sandstone columns for chemical durability tests

column	height	mass of sand	volume	dry density	matrix volume	pore volume	porosity	hight precipitated
	h	m	V	ρ_{dry}	V_{matrix}	V_{por}	Φ	$h_{perc.}$
	[cm]	[g]	[cm^3]	[cm^3]	[cm^3]	[cm^3]	[%]	[cm]
CR 1	16	844.4	539.13	1.57	324.77	214.36	39.76	11.5
CD 2	16	879	539.13	1.63	338.08	201.05	37.29	12.0
CD 3	16	894.9	539.13	1.66	344.19	194.94	36.16	12.2
CR 4	16	865.1	539.13	1.60	332.73	206.40	38.28	11.8
CB 5	16	876.5	539.13	1.63	337.12	202.01	37.47	13.5

3.2 FLUSHING PROCEDURE

As previously stated all five columns were made in an identical way leading to the assumption of the same properties. Thus one of the columns was not flushed at all but left blank in order to compare its strength with the strength of the flushed columns.

For better comparison both experimental parts, the flushing and data collection with demineralized water and artificial rain water was done according to the same procedure. The flushing of the columns was done from top to bottom with a flow rate of 200ml/h, which makes for approximately 1PV/h for a time of 10 days, flushing each column with 260 times the pore volume. Samples of the influent as well as the effluent were taken twice a day measuring the conductivity, pH and $CaCO_3$ content. For practical reasons the flow rate had to be decreased to half the speed during the time of the weekends.

The demineralized water was sparged with nitrogen in order to prevent the dissolution of carbonate into the fluid keeping its concentration in the influent at a minimum. Previous to flushing the rain water was artificially created in the lab, using averaged compounds and its amounts (RIVM Rapport 723101046, Landelijk Meetnet Regenwatersamenstelling, April 1999). The exact composition of the artificial rain water as it was made can be seen in table 3.2. Ideally the pH of the water was kept between 5 and 6 throughout the duration of the experiment. The artificial rain water was stored in a conventional vessel with only a loose lid as being used for flushing. That way carbonate could dissolve into the surface of the fluid, thus mimicking real rain water traveling through the atmosphere and percolating through the soil.

TABLE 3.2: Composition of the artificial rain water

Salts	mg/L
$(NH_4)_2\ SO_4$	8.8268
$MgCl_2$	1.5044
$CaNO_3$	0.6665
KNO_3	0.6125
$NaHCO_3$	0.4550
NaCl	1.3189
K_2HPO_4	0.7481
NH4Cl	0.0523
$NaNO_3$	7.8413

3.3 RESULTS AND DISCUSSION

The obtained experimental data clearly shows a decrease in compressive strength of all treated samples which can be related to dissolution processes inside the samples. During the measurements throughout the course of the experiment it was observed, that pH, conductivity and CaCO3 content increased after passing the cemented samples. This development shows that some kind of dissolution reactions must have taken place as the fluids were flushed through the samples. Since the aim of this study was to determine the loss of strength due to chemical alteration caused by pore fluids, the exact circumstances and

chemical processes that obviously took place inside the material were not investigated. However the $CaCO_3$ content is clearly an important factor of the strength of calcareous soils therefore its dissolution was taken more under consideration and will be discussed in the following.

3.3.1 EFFECTS OF DISSOLUTION

The measurements of $CaCO_3$ content show a clear increase in the amount dissolved in both flushed through fluids. From the data it is rather hard to distinguish which fluid had the greater impact on the material, since all values are more or less in the same range, however the values of the artificial rainwater show a higher scatter. An average dissolution rate of $CaCO_3$ was estimated for each column. For the artificial rain water the dissolution rates of $CaCO_3$ can be approximated by about 10 mg/L with a rather high standard deviation (detailed values are given in table 3.3). This rather high scatter of dissolution might be due to the fact that the fluid had to be artificially created in the lab in 4 separate batches, which can lead to slight differences in composition. Another possible factor that could have caused the scatter of the measured data is the fact that the vessel in which the influent was stored in was not constantly stirred. By measuring the pH at the top and at the bottom of the vessel it was discovered, that a gradient in pH has formed along the depth of the fluid, with high values at the top and lower values at the bottom of the vessel. This fact leads to the assumption that also a gradient in $CaCO_3$ content and others might have formed. The demineralized water shows a bit lower dissolution rates in the range of approximately 7 mg/L. Here the standard deviation was on a much lower level. As stated in table 3.3 and illustrated in figure 3.2, after flushing the columns with 260 pore volumes of fluid, the total dissolution of $CaCO_3$ was able to be estimated to 3-4.5 % of the initial amount $CaCO_3$.

TABLE 3.3: Details of dissolution

CaCO3		**CR 1**	**CR 4**	**CD 2**	**CD 3**
dissolution rate	[mg/L]	9.97	9.12	7.08	6.62
standard deviation	[mg/L]	2.42	2.42	2.42	2.42
density after treatment	[mg/cm³]	30.5	40.2	30.0	29.8
total amount after treatment	[g]	11.82	15.98	12.13	12.25
initial density	[mg/cm³]	31.93	41.43	30.92	30.62
initial content	[g]	12.373	16.472	12.500	12.586
total amount dissolved	[g]	0.555	0.488	0.370	0.336
	[%]	**4.48**	**2.97**	**2.96**	**2.67**

As already stated earlier due to practical reasons the flow rate had to be lowered by half two times during the course of the experiment each time for approximately 65 hours. However this should not be taken as a short coming because the decrease gave an additional degree of freedom to the experiment. But as can be seen from figure 3.3 the dissolution of $CaCO_3$ remained unaffected, which indicates that obviously the full capacity of dissolution is already being reached at the flow rate of 1PV/h.

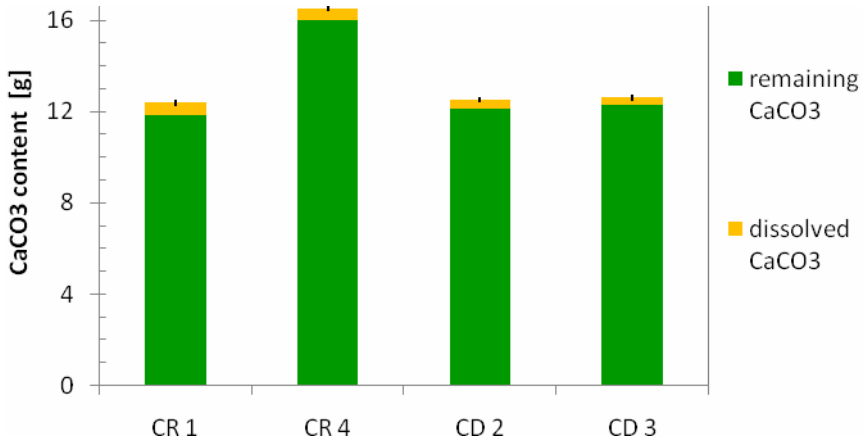

FIGURE 3.2: Initial $CaCO_3$ content of all samples with total amount of dissolved and remaining $CaCO_3$ content, with indicated standard deviation.

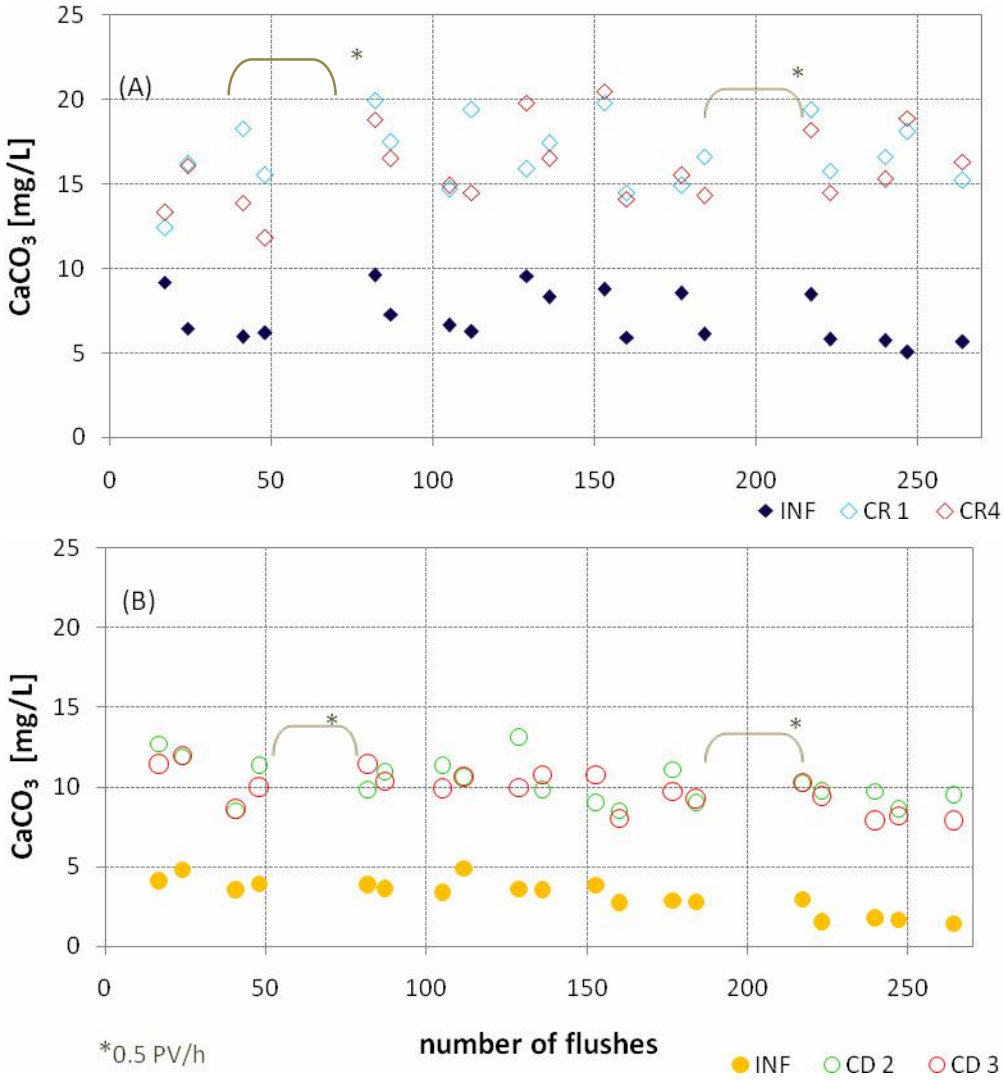

FIGURE 3.3: Dissolution of $CaCO_3$ content for flushed through artificial rainwater (A) and demineralized water (B) plotted throughout the time of the experiment; the intervals marked with * indicate the period of lower flow rates during the weekends (0.5 PV/h)

After the process of flushing the columns was completed the precipitated sand bodies were excavated from the PVC tubes and their unconfined compressive strength tested. Due to the insufficient height of the samples the UCS tests had to be carried out on a 1:1 ratio and back calculated to standard values of 1:2 ratio according to ASTM D2938-86. All details of the tested sand samples can be seen in table 3.4.

As previously stated CB5 was intentionally left blank and not flushed in order to estimate the residual strength of the precipitated sand bodies after treatment. Also the correlation with dry density and peak strength was established as shown in figure 3.4. It can be seen from the plot that all samples are below the estimated strength levels, also CB5 which indeed should correlate with the predicted strength since it was not treated. The smaller real strength of the sample is most probably due to the lower content of $CaCO_3$. As is shown in table 3.2 the initial content in S5 is the lowest of all samples tested even taking the dissolution of the treated columns into account. The cementation correlated with the dry density determines the strength of the material, but the correlation shown in fig 3.4 does not take into account the $CaCO_3$ content this might have caused this incoherence. Since both values of CB5 are very low compared with the treated samples it is understandable that its strength ranges around the same values as the treated samples.

TABLE 3.4: Details of precipitated sand columns prepared for unconfined compressive strength tests.

		CB 5	CR 1	CR 4	CD 2	CD 3
h_{prec}	[cm]	13.5	11.5	11.8	12	12.2
h	[cm]	5.37	5.25	5.44	5.15	5.23
d	[cm]	6.55	6.55	6.55	6.55	6.55
m	[g]	374.8	357.9	388.7	356.2	355.2
V	[cm³]	180.9	177.1	183.4	173.6	176.2
V_{mat}	[cm³]	122.3	118.2	129.8	119.7	118.9
m_{dry}	[g]	318.0	307.3	337.5	311.3	309.2
m_{sat}	[g]	376.6	366.2	391.1	365.2	366.5
V_{water}	[cm³]	58.59	58.91	53.59	53.87	57.30
ρ_{dry}	[g/cm³]	1.76	1.74	1.84	1.79	1.75
	[mg/cm^3]	26.00	30.50	40.20	34.00	29.80
$\mathbf{q_1}$	[kPa]	695	1034	1269	966	989
$\mathbf{q_{0.5}}$	[kPa]	593	877	1086	815	838
$\mathbf{q_{pre}}$	[kPa]	1333	1163	2184	1647	1306

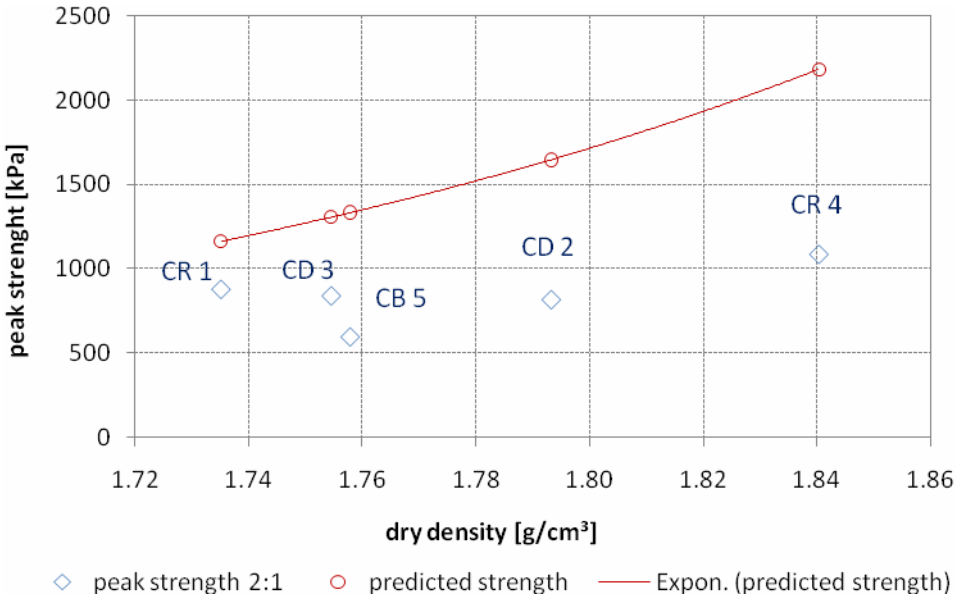

FIGURE 3.4: Predicted strength with respect to dry density calculated according to van Paassen (2009) and measured peak strengths of the treated samples.

The key part of the carried out experiment is also to establish a correlation between the loss of $CaCO_3$ and the degradation of strength due to this. Although tables 3.3 and 3.4 indicate a correlation that with increasing amount of dissolved $CaCO_3$ the loss of strength is decreasing, the data available is not sufficient enough in order to establish a sophisticated correlation, especially if we take the samples CR1 and CD3 into consideration. Table 3.3 shows that CR1 encountered the highest total amount of dissolution, whereas CD3 showed a minimum loss in $CaCO_3$. Yet CR1 shows a similar decrease in strength as CD3.

3.4 CONCLUSION

The performed test gave first experimental results on strength degradation of BioGrout due to chemical alteration caused by pore fluids. By flushing demineralized water as well as artificial rainwater through BioGrout samples a slightly varying but over all constant dissolution of cementing material was found. One blank sample of the same series and the correlation between dry density and peak strength allowed for estimations of unconfined compressive strength before the treatment. The UCS test showed a decrease in peak strength from the expected values. Yet no substantial correlation between the loss of $CaCO_3$ and decrease in strength could be established.

Taking into account only the absolute values obtained from the performed experiment an aquifer consisting of BioGrout with an average ground water flow of 1m per day would encounter a loss of only 0.01% $CaCO_3$ in 50 years considering the fluid passing through the material had the same properties as the used demineralized water.

3.5 OUTLOOK AND REMARKS

The carried out experiment on the durability of BioGrout towards chemical alteriation through pore fluids provides a first insight on the relationship between dissolved $CaCO_3$ and degradation of strength. The results clearly indicate a correlation of these two; however for a substantial calculation of the correlation further experiments should be carried out with a larger number of samples.

Other aspects of interest which were omitted in this work are the chemical processes that are obviously going on as the fluid is being flushed through the material. Further investigations regarding this aspect could give a better understanding to the overall chemical durability of the material.

Considering the flushing of the BioGrout columns one important remark should be mentioned here. As already mentioned in chapter 3.3 the storage vessel for the influent of the artificial rain water was not stirred continuously which caused gradients to form along the depth of the fluid. This might have caused part of the scatter in the data. In order to prevent this from happening the liquid should be stirred constantly.

4 FREEZING- THAWING CYCLES

For use of BioGrout as ground improvement material in the more shallow subsurface the material might encounter effects of changing weathering conditions that might alter its compressive strength. There are three generally accepted physical processes that can diminish the strength of building materials, which also can account for BioGrout: these are heating and cooling, wetting and drying, and freezing and thawing. As Hale and Shakoor (2003) reported the effects of heating and cooling as well as wetting and drying were not found to have a reducing affect on the strength of the sandstones they have tested. Only the freezing and thawing cycles showed significant effect on the degradation of strength. Hence in the following only the effect of freezing and thawing cycles on BioGrout will be briefly examined.

Since yearly cycles of temperatures well below and above zero can cause cycles of freezing and thawing of the materials pore fluids. Thus the expansion and subsequent contraction of the pore fluids might cause cracks inside the material weakening it. This degradation of strength can be crucial for the final application of BioGrout as ground improvement material.

4.1 MATERIAL

The freeze- thaw cyclic experiment was performed on samples from the second field scale experiment at Papendrecht. The cores, from which the samples were cut, were drilled form the same block as those subjected to cyclic loading. The locations of the samples are indicated in picture 2.1.

4.2 PROCEDURE

In order to determine the residual strength of the cores after the treatment again the correlation of van Paassen (2009) was used.

Prior to testing the samples were stored in water in order to obtain a high water content and then wrapped into foil to prevent loss of water and sand grains from the surface of the cores during testing.

The freezing- thawing treatments were carried out in a conventional freezer with a constant temperature of -18°C. The thawing cycles of this experiment were conducted in a warm water bath with a of temperature 20°C. Both samples were subjected to 26 freeze-thaw cycles, with duration of 16h and 8h respectively. After completion of this part of the test the unconfined compressive strength of the samples was tested. During handling the samples after the freeze- thaw cycles S06 broke in half and therefore had to be tested with a 1:1 ratio, S10 was intact and therefore tested on standard 1:2 ratio.

4.3 RESULTS AND DISCUSSION

During the freeze- thaw cycles it was observed that in both samples some sand grains were crumbling of the surface of the core, despite the foil wrapped around. As the pore fluids freeze concentrically towards the inside of the core the expansion of the fluid can cause some grains at the very surface to break off easier. However this effect is only expected to occur at the very surface of the material. Due to this fact the dimensions of the samples decreased slightly after the treatment as can be seen in table 4.1.

As already mentioned above S06 broke at the middle with a more or less even plane during handling after all freeze thaw cycles were completed. Signs of weakening or cracks could not be observed earlier. The failure of the sample most probably occurred due to inhomogeneity of the sample.

Table 4.1 shows the measured unconfined compressive strength of both samples. The correlation of dry density and peak strength by van Paassen (2009) show a decrease in strength for S10 by approximately 170kPa. However for S06 the strength predicted is lower than the actual strength by 26kPa. This might be within a range of error of measurements and prediction as well as further inhomogeneity of the tested part of the core.

TABLE 4.1: Details of samples before and after freeze- thaw cycles as well as peak strength measured during UCS test.

			S10	S06 *
before treatment	d	[cm]	6.42	6.40
	h	[cm]	13.20	13.56
	m	[g]	876.1	853.9
after treatment	d	[cm]	6.41	6.38
	h	[cm]	13.19	13.50
	m	[g]	874.3	841.2
	ρ_{dry}	[g/cm³]	1.88	1.66
	ϕ	[%]	0.231	0.232
	CaCO3	[mg/cm³]	62.47	40.30
	q_{pre}	[kPa]	2824	759
	q	[kPa]	2657	785

4.4 CONCLUSION

In the carried out freeze- thaw cycles in regard to degradation of compressive strength of BioGrout it was found that there is a clear effect of strength loss due to the freezing and thawing. However for more reliable and specific results and correlations further experiments with a larger number of samples should be carried out.

ACKNOLEDGEMENTS

This work is part of a research project performed by Deltares. Special thanks to Marien Harkes and Wouter van de Star for their support and help in the lab work.

LITERATURE

BOSCHLOO, D.J., STOLK, A.P.: Landelijk Meetnet Regenwatersamenstellingen, Meetresultaten 1995. *(1999) RIVM Rapport 723101046 Rijksinstituut voor volksgezondheid en milieu national institute of public health and the environment.*

HALE, P.A.; SHAKOOR, A.: A laboratory investigation of the effects of cyclic heating and cooling, wetting and drying, and freezing and thawing on the compressive strength of selected sandstones. *Environmental & Engineering Geoscience, Vol. IX, No. 2, (2003), pp. 117-130.*

HARKES, M.P., et al.: Fixation and distribution of bacterial activity in sand in induced carbonate precipitation of ground reinforcement. *Ecol. Eng. (2009), doi10.1016/j.ecoleng.2009.01.004*

LO PRESTI, D.C.F., et al: Shear modulus and damping of soils. *Géotechnique, 47(3) (1997), pp. 603-617*

O'REILLY,M.P., BROWN,S.F.: Cyclic Loading of Soils: from theory to design. *(1991) Blackie and Son Ltd*

VAN PAASSEN, L.: BioGrout. Ground improvement by microbially induced carbonate precipitation. *(2009) Delft University of Technology*

SHARMA.,S.S, FAHEY, M.: Deformation characteristics of two cemented calcareous soils. *(2004) Canadian Geotechnical Journal: (41):1139-1151*